JAAS

ROYAL SOCIETY OF CHEMISTRY

PAPER

View Article Online
View Journal | View Issue

Check for updates

Cite this: *J. Anal. At. Spectrom.*, 2025, **40**, 238

Simultaneous multi-angle AR-XANES for surface-sensitive chemical speciation of gold nanolayers in wall painting replica†

Maram Na'es, *[a] Lars Lühl,‡[a] Daniel Grötzsch,[a] Ioanna Mantouvalou, [ab] Jonas Baumann §[a] and Birgit Kanngießer[ab]

Received 25th July 2024
Accepted 13th November 2024

DOI: 10.1039/d4ja00269e

rsc.li/jaas

Wall paintings from the world heritage site Petra-Jordan contain gilding remnants, which show various types of degradation. To investigate the deterioration processes as well as assess the conservation treatment, non-destructive (ND) and non-invasive (NI) analyses of the chemical species of gold are mandatory. In this work, simultaneous multi-angle angle-resolved X-ray absorption near-edge spectroscopy (AR-XANES) measurements were performed to assess gold species variations in depth. Experimental validation proved the method to be successful in differentiating between gold species in nanolayered structures. Technical advantages and limitations of the method are discussed. The application of a conservation material containing Nano Gold Gel (NGG) applied underneath a gold layer to regenerate adhesion with its support layer was also examined.

Introduction

Gilded wall paintings and stucco often undergo various deterioration processes. Especially gold delamination due to binder aging and loss is a common phenomenon.[1] One typical conservation treatment is the overlaying of the original gold layer with a new gold leaf or powder fixed by an organic binder. The elemental composition of commonly used commercial gold conservation materials shows a high copper and silver content,[2] which is not recommended due to its reactivity with chloride and sulfate ions in the surrounding environment. This leads to accelerated chemical degradation of the gold layer, which is unwanted in a conservation process.[3,4] Therefore, new conservation protocols and materials need to be considered.

In the case of gold delamination, a powder form of gold mixed with a compatible binder to be delivered to the delaminated gold layer or to fill the gaps in the cracks of the gold layer is a viable solution. Therefore, Nano Gold Gel (NGG) composed of gold nanoparticles (AuNPs) stabilized with natural organic polymers compatible for gold layer conservation in gilded painted surfaces was synthesized, as described in detail in ref. 2 and 5.

AuNPs in the NGG compensate for the gold's mass loss in the historical gold layer. They also increase the lifetime of the natural polymer adhesive used to stabilise them.[6,7] The antibacterial properties of AuNPs[8] are an advantage, especially if the painting is at risk from bacterial infestation. The application of NGG on replica samples allowed us to understand its interaction with individual layers of the gilded structure.[5] In a real wall painting, paint and gold surfaces are layered. Thus, for assessing the performance of NGG as a conservation material for gilded painted surfaces, non-destructive (ND) and non-invasive (NI) methods for in-depth chemical speciation at the nanometer scale are needed. Achieving this while maintaining good analytical resolution remains challenging due to surface roughness, relative low concentration of the NGG, and absorption effects.

For cultural heritage materials, the highest priority is not to be damaged or altered during an investigation. Additionally, when using X-rays, a highly efficient methodology is necessary for the reduction of Au species to metallic Au. However, the use of X-ray radiation induces photo-reduction of oxidised gold species. Such photo-induced chemical change was also noticed by Harada (2016).[9] Therefore, using a highly efficient methodology with short measurement times is desirable. Chemical changes at the surface and interfaces are usually investigated by examining chemical speciation in 2D and 3D. The commonly used ND technique for chemical speciation of layered cultural heritage (CH) objects is two-dimensional mapping using conventional Micro X-Ray Absorption Near-Edge Spectroscopy (μXANES) on a cross section from the object.[10–18] This requires invasive sampling before the non-destructive μXANES analysis is performed. Three-Dimensional Micro X-Ray Absorption Near-

---

[a] *Institute for Optics and Atomic Physics, Technical University Berlin, Hardenbergstr. 36, 10623 Berlin, Germany. E-mail: maram@physik.tu-berlin.de*

[b] *Helmholtz-Zentrum Berlin für Materialien und Energie, Albert-Einstein-Str. 15, 12489 Berlin, Germany*

† Electronic supplementary information (ESI) available. See DOI: https://doi.org/10.1039/d4ja00269e

‡ Current address: Pfeiffer Vacuum GmbH, Germany.

§ Current address: Bruker Nano GmbH, Am Studio 2D, 12489 Berlin, Germany.

Edge Structure (3D-μXANES) is another method used for the identification of painting materials in historical wall paintings and glazed ceramics.[19–21] This method is NI and ND, but in the case of gold as the analyte and concerning the composition and concentration of the NGG experimental conservation material, some issues arise. First, the high self-absorption in the material (gold) distorts the XANES data. Second, due to low efficiencies for nanolayers, very long acquisition times are needed to detect NGG nanocomposites in depth. Third, the depth resolution of conventional and confocal μXANES for gold, which is in the tens of micrometer range, is insufficient. Even if the first challenge can be overcome with acceptable impact on spectra after spectral correction, the second causes irreversible photoinduced reduction of gold species, resulting in 100% metallic gold after long exposure time. This means, if gold changes its oxidation state upon interaction with interfaces, it cannot be investigated using this method. To overcome the third challenge of depth resolution, a highly efficient ND and NI angle-resolved μXANES setup in grazing emission (GE) geometry (AR-μXANES) is used and tested as a proof-of-principle. Recently, Çakir *et al.* (2023)[22] combined Angular Resolved X-Ray Fluorescence (AR-XRF) and pnCCD detectors to perform AR-XANES, investigating the corrosion processes in compositionally complex alloys. Orsilli *et al.* (2023)[23] studied AR-XRF of gold nanolayers using an SDD detector with one vertical slit in front.

An application of our setup on the synthesised NGG as an experimental gold conservation material is presented. The combination of μXANES analysis and GE geometry allows differentiation between chemical species of the same element (*i.e.* variable oxidation states) at surface and near-surface layers with reasonable measurement time. The GE geometry maximizes the signal originating from the surface and near-surface layers while reducing background contributions. For samples with smooth interfaces, the depth-resolving capabilities of the method are drastically increased due to interference effects.[24,25] However, for CH samples a well-defined smooth surface is usually not at hand, and thus the implications due to the critical angle are less strict. Still, the prolonged path lengths at shallow detection angles lead to signal-to-background enhancements, too. Moreover, a GE setup allows the use of focused synchrotron radiation for excitation, enabling increased lateral resolution.[26]

Unlike Total Reflection X-Ray Fluorescence (TXRF),[26–28] self-absorption effects which distort the XANES spectrum are expected to be minimal in AR-XANES in the GE geometry. This is due to the minimized path length of the incident beam contributing to the detected XRF signals through the sample.[26] AR-XANES is directly applied on the object allowing a non-invasive sampling and a non-destructive investigation.

Often, AR-XRF in the GE mode is performed with an energy-dispersive detector in a scanning mode, such as a silicon-drift detector (SDD), with a slit in front for increased angular resolution.[23,25,29] Here the efficiency of the setup is poor due to the very limited solid angle of detection. Alternatively, scanning-free approaches are used, where the detector is a 2D pixelated detector enabling a large solid angle of detection while keeping a good angular resolving power.[22,30] While in this scheme no scanning is necessary, the data evaluation can be cumbersome and typical count-rates of, *e.g.* CCD cameras, are limited due to the necessary operation in single photon counting mode. We present an AR-XRF setup that combines advantages of both scanning and scan-free approaches for maximal efficiency. A 7-element SiLi detector with a specially designed multi-slit system enables a suitably large solid angle of detection simultaneously, while posing all the advantages of well-established energy-dispersive detectors. What is aimed to be investigated here is whether a chemical alteration of gold at the surface and interface layers occurs due to the use of the experimental conservation adhesive.

While testing the method on an actual historical sample would be beneficial, current work was applied on lab replicas only for ethical reasons in accordance with Article 5 of ICOMOS 2003 Principles for the Preservation and Conservation-Restoration of Wall Paintings, specifically the long-term effects of new materials and methods on wall paintings, which are unknown and could be harmful.[31]

Materials and methods

Synthesis of experimental gold conservation material (Nano Gold Gel (NGG-1b))

Gold nanoparticles (AuNPs) were synthesised using $HAuCl_4 \cdot 3H_2O$ as a gold precursor and gelatin as a reducing and stabilizing agent. From a freshly prepared gelatin solution of 3.3%, 5 mL was added to 5 mL (10 mM) $HAuCl_4 \cdot 3H_2O$. The solution was vigorously and continuously stirred at 80 °C till pink color formation. The synthesised adhesive (NGG-1b) was purified by a double centrifugation process. The final supernatant was decanted and disposed, and the NGG part was redispersed in 0.5 mL gelatin and stored at 4 °C in a fridge. Stoichiometric calculation of gold weight in the synthesised NGG is 9.8485 mg. The average particle size of NGG-1b is (38 ± 5) nm, as characterised by transmission electron microscopy.[5]

Preparation and characterisation of reference and replica samples

Two sets of samples were prepared for AR-XANES measurements. The first is a reference layered sample (R1) and the second is a replica sample (S1), where NGG-1b is applied (see ESI, Fig. S1†). The reference sample was prepared by mixing 20 mg Au_2O_3 (density 11.34 g cm^{-3}) and 1 mg Fe_2O_3 (density 5.24 g cm^{-3}) with a matrix of 80 mg cellulose (±1 mg). The mixture was placed in a manual press container and a 1 cm × 1 cm gold leaf (200 nm, 19.32 g cm^{-3}, Kremer Pigmente GmbH & Co., ID 98412) was cut and placed over the mixture, and then they were pressed together using a manual hydraulic press to produce a 13 mm-diameter and a 3 mm-thick pellet. For the replica sample, a gypsum (Sigma-Aldrich, ID 12090) support pellet was first prepared and left until complete dryness. Then a layer of α-Fe_2O_3 (Kremer Pigmente GmbH & Co., ID 48120) was applied with the aid of water generating an approximately 300 nm-thick layer. Finally, a 1 cm × 1 cm gold leaf (200 nm, 19.32 g cm^{-3}, Kremer Pigmente GmbH & Co., ID 98412) was placed atop before complete dryness of the layer. The sample

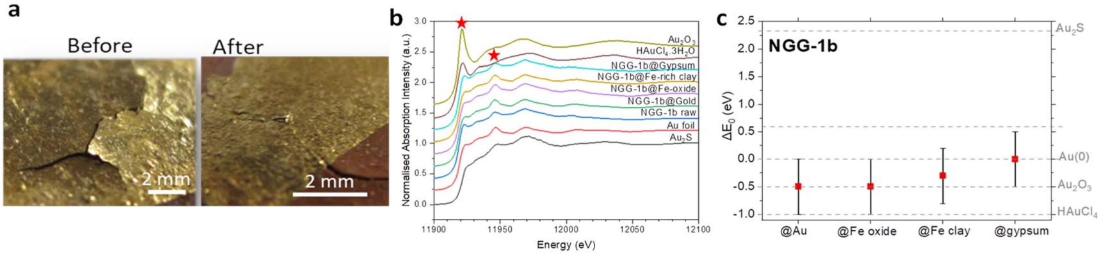

Fig. 1 (a) Replica sample before and after the application of NGG. (b) XANES spectra of Au(0, I, and III) reference compounds and NGG-1b raw and applied over various surfaces, see ESI† for XANES settings. All spectra were recorded at $\theta_E = 45°$ and read from the central detector D2. (Savitzky Golay smoothing, 4th polynomial order, 10 points widths). Characteristic energies for Au(III) at 11 922.5 eV and Au(0) at 11 948.5 eV are marked with asterisks. (c) Shift of the absorption edge energy for applied NGG-1b over the four studied surfaces in reference to raw NGG-1b. The edge energy of the gold standards is marked in horizontal dashed grey lines.

was then artificially aged (see ESI†) to de-stabilise the bonding of the gold layer. Subsequently, NGG-1b (1.742 g cm^{-3}) was applied in delaminated gilded areas to restore bonding (Fig. 1a). Prepared reference and replica samples were examined by Micro X-Ray Fluorescence (μXRF) spectroscopy[32] from the surface side and on a cross section. Detailed examination results can be found in ESI, Fig. S10–12.† Surface irregularities and roughness were evident and unfortunately unavoidable. These irregularities have made the AR-XANES measurements a great challenge.

To correctly evaluate the chemical behaviour of NGG-1b applied between the gold and iron oxide layers, it was necessary to first evaluate its interaction at individual layers of the gilded structure. A 100 μL drop of NGG-1b was deposited each on a Doppel gold leaf (Kremer Pigmente GmbH & Co., ID 98412), on α-Fe_2O_3 (Kremer Pigmente GmbH & Co., ID 48120), on Fe-rich clay (SRM 679, NIST), and on gypsum (Sigma-Aldrich, ID 12090) to resemble paint, mordant, and preparation layers, respectively, of the gilded structure. Conventional XANES analysis (see ESI†) was then performed on all four samples. Spectral features of the applied NGG-1b differ from its pure form, as shown in Fig. 1b and c indicating a possible chemical change of gold upon interaction with the surface. This motivated us to investigate the possibility of detecting a chemical change of gold, ND and NI using a surface-sensitive method, at the interfaces of a layered structure composed of the same individual layers.

XANES spectra for reference gold compounds shown in Fig. 1b were recorded in transmission and fluorescence modes for GoodFellow® gold foil (5 μm), pellets of gold oxide Au_2O_3 (20 mg in 80 mg cellulose), pellets of chloroauric acid $HAuCl_4 \cdot H_2O$ (30 mg in 80 mg cellulose), and pellets of gold sulfide Au_2S (20 mg in 80 mg cellulose). The same XANES settings used for the above-mentioned NGG-1b experiment were used here. Reference gold compounds were prepared for the identification of gold ionisation through Linear Combination Fit (LCF) performed using the ATHENA program.[33] Table S2† lists the main characteristic XANES peaks for reference gold compounds used in this work.

AR-XANES setup

Experiments were performed at the synchrotron radiation source Bessy II of the Helmholtz-Zentrum Berlin (HZB) at the MySpot beamline.[34,35] The experimental setup and fundamental arrangement are shown in Fig. 2a and S2 (ESI†). A Si(311) double-crystal monochromator allowing an energy resolution of $E/\Delta E = 10\,000$ at the measured energy range (11 900–12 400 eV) was utilized. The incident X-ray intensity was monitored using an ionisation chamber. The excitation beam was focused using a polycapillary half lens (focal distance 40 mm) allowing a beam spot size of 30 μm FWHM at the sample position for the energy region around the copper K-edge (8959–9023 eV). A 7-element Si(Li) detector (Gresham Scientific Instruments) was used to collect emitted fluorescence radiation at 90° from the excitation beam. The effective detection area of each detection window of the 7-element detector was reduced by a specially designed slit-cap placed at the detector head, allowing better angular resolution of the emitted fluorescence at GE angles (Fig. 2 and ESI, Fig. S2†). The slit-cap arranges the seven-element detector windows into three vertical detector arrays (highlighted yellow in Fig. 2b) with three distinct detection angles (Fig. 2b). Fluorescence intensities detected at vertical detector arrays were normalised to the excitation intensity (derived by the ionization chamber signal) and the detector lifetime and then averaged. During measurements, the detector was kept in a fixed position, while the sample stage was rotated (Fig. S3†). The sample-to-detector distance was 40 mm. The 7-element detectors were numbered from 2 to 8, as sketched in Fig. 2.

Experimental procedure

Determination of the surface angle. The surface angle for every sample and position was manually determined due to surface imperfections in terms of flatness. With an excitation radiation well above the absorption edge of Au L_3 (12.1. keV), each sample was scanned (from −2° to 10° with 0.1° step size, 5 seconds per step) and the Au-$L_{\alpha 1}$ fluorescence intensity (ROI: 930–1050) was monitored in reference to the central detector. The surface angle is defined as the angle where the fluorescence intensity curve starts to increase, see explanation in the ESI (Fig. S4†). Filters were employed when the dead time of the detectors exceeded 30% (ESI, Table S1†).

Correlating measured depth to measuring angle. Correlating the information depth of the X-ray beam with exit angles of detection is essential to understand the source of information read using the detector at each exit angle. The information

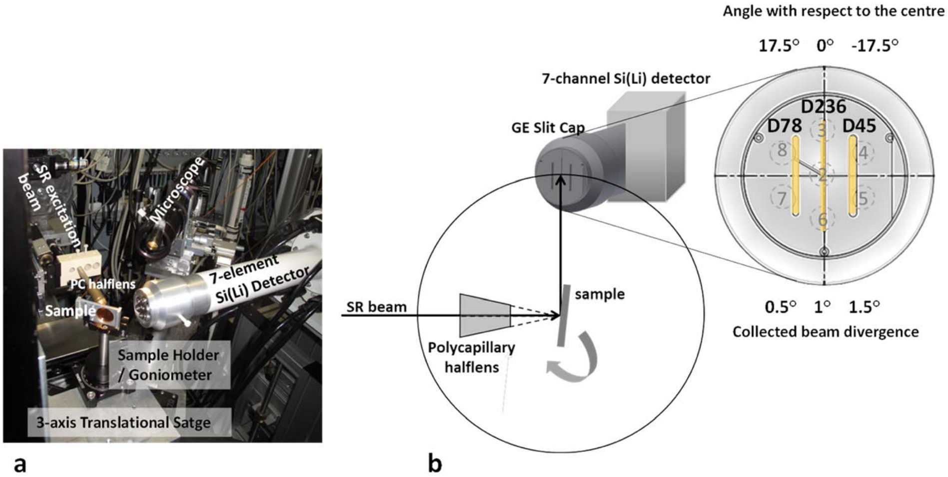

Fig. 2 (a) Photo of the experimental setup at the MySpot beamline. Note the detector was photographed before the GE slit cap was added. (b) Experimental arrangement of AR-XANES/AR-XRF measurements collected in fluorescence mode. The detector was kept at a fixed position, while the sample stage was rotated. An illustration of the slit-cap and numbering system used for the 7-detectors and the three detector arrays are shown.

depth of the X-ray beam in a material can be described as the depth, from which still more than 36.7% ($1/e$) of the created fluorescence intensity originates. In our case, due to the shallow emission angles θ_E, the attenuation of the XRF signal dominates and the information depth can be approximated by $d_{1/e} = \sin(\theta_E)/(\mu_i\rho_i)$, with μ_i the attenuation coefficient of a layer i with density ρ_i for the energy of the detected Au L_3–M_5 fluorescence (9.713 keV). This is calculated[36] for Au, Au_2O_3, and NGG and shown in Fig. 3. At 90° incident angle, the detection angle is close to 0° with respect to the sample surface and thus the information depth and the XRF signal are minimal. When the sample is tilted during the angular scan, the exit angle increases gradually, leading to an increase in the information depth. The interface layer at around 200 nm depth is the area where the gold leaf layer ends and $Au_2O_3 + Fe_2O_3$ for R1 starts, and the Au/NGG/Fe_2O_3 interface layer for replica sample S1 starts. This is the region of interest because it bears the chemical features of NGG-1b interaction with the gold surface layer and the iron oxide layer. As can be seen, only after an emission angle of about 2° the fluorescence radiation on the way to the detector can transmit through the gold foil layer and the signal starts to originate significantly from the Au–Fe_2O_3 interface layer.

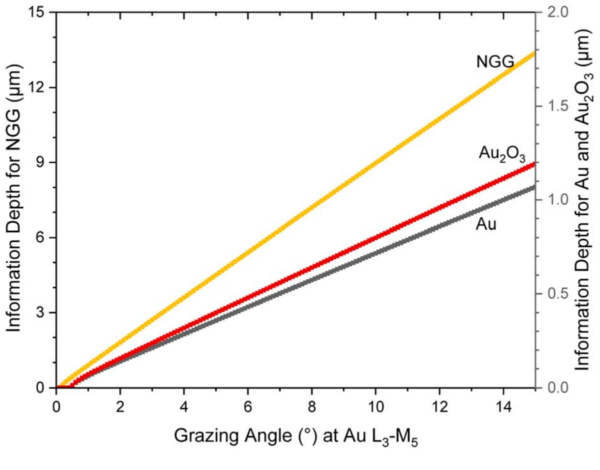

Fig. 3 Information depth at various exit angles for Au, Au_2O_3, and NGG at Au L_3–M_5 fluorescence line calculated from CXRO website[36] [last accessed 24.06.2024].

AR-XANES and AR-XRF measurements. AR-XANES measurements were performed by fixing the exit angle θ_E and varying the excitation energy E_0. The sample was fixed initially at the zero position and XANES scans were performed with 11 s per step acquisition time. Four different energy regions with varying step sizes were investigated (10 eV @ 11 800–11 900 eV, 0.5 eV @ 11 890–11 960 eV, 1 eV @ 11 959–12 100 eV, 10 eV steps @ 12 000–12 400 eV). This procedure was then repeated for 8 further sample rotation positions with 5° step size up to 45°. XANES spectra were normalized to the excitation intensity from the ionisation chamber and the detector's lifetime was then processed using the standard normalization and background correction procedure of the ATHENA program.[33] AR-XANES spectra were visualized using Origin (version 2021).

AR-XRF profiles were extracted from the AR-XANES spectra at the three characteristic energies for gold representing Au(0) and gold(III) oxide species at 11 948.5 eV and 11 922.5 eV, as marked in Fig. 1b, respectively, as well as a total gold signal at 12 100.0 eV. In contrast to this, the ATHENA background correction was not applied, since all additional absorption was included in the subsequent analysis using C++ and Python-based in-house software for fundamental parameter fluorescence calculation.

Results

Depth-resolved chemical speciation using energy scans at fixed exit angles

The angular dependence of Au L_3 AR-XANES spectra for the reference (R1) and the replica (S1) sample are plotted in Fig. 4a and b, respectively. A schematic illustration depicting the

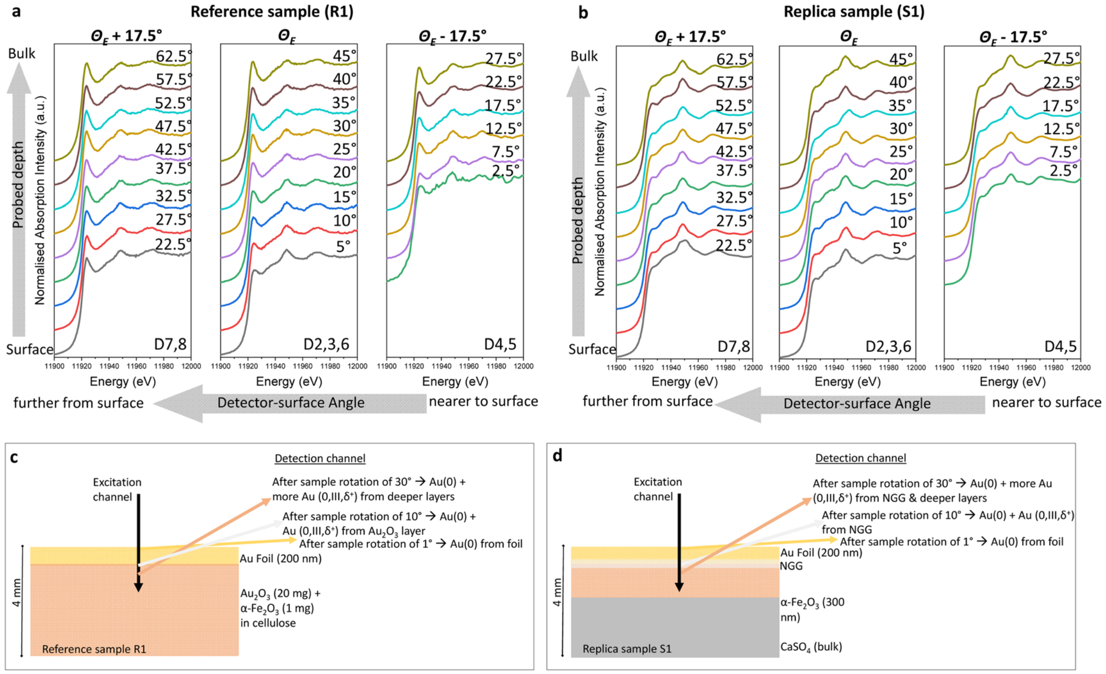

Fig. 4 Normalized AR-XANES spectra for (a) reference sample R1 and (b) replica sample S1, at all measured exit angles as read from the three sets of detector arrays. (c) Schematic depicting information depth at various exit angles of detection for reference sample R1 and (d) replica sample S1.

general expected signal contribution at various depths seen from various exit angles of detection for both reference and replica samples is shown in Fig. 4c and d, respectively. Furthermore, correlating AR-XANES results of S1 and µXRF elemental maps on its cross section are shown in ESI Fig. S8 and S9.† Qualitatively, the white line intensity of R1 increases gradually from shallow exit angles of detection (Fig. 4a, bottom) towards higher exit angles (Fig. 4a, top). This is in good agreement with the expected increased contribution of the bulk signal containing Au(III) oxide. This spectral change confirms that the employed setup and the measuring method work. However, it is apparent that in the resulting AR-XANES spectra, in the case of gold(0) and gold(III) oxide, this method is qualitatively unable to resolve a signal from the upper 200 nm Au alone. Even at shallow angles of detection, Au(III) oxide is also detected. This is in good agreement with the calculated angular-dependent information depths, as shown in Fig. 3, from which we see that for emission angles >2.5° the information depth in Au already surpasses the 200 nm of the Au foil, allowing signal contribution from the substrate and interface layers. Indeed, it can even be expected that even for more shallow angles, a substrate signal can still be detected, since the samples showed already by visual inspection surface irregularities like roughness and discontinuities. This already indicates the difficulties regarding possible quantitative information to be gained from the measurements.

The recorded spectra at the three sets of detector arrays for the replica sample S1 presented in Fig. 4b show comparable behaviour. It is difficult to detect a significant change using this qualitative assessment approach, therefore two quantitative approaches of LCF using ATHENA(33) and intensity ratios at marker energies of the AR-XANES spectra at all detectors and measured exit angles were performed for both samples.

Reference spectra shown in Fig. 1b were employed in the fit in addition to the experimental conservation material NGG-1b in the case of the replica sample. The results for R1 and S1 are shown in Fig. 5a and b, respectively. For reference sample R1, as the angle of detection increases, a decreasing trend of Au(0) signal and an increasing Au(III) signal can be seen in Fig. 5a. A similar trend is also seen in the decreasing contribution of Au(0) weight percentage and the increasing contribution of Au(III) in relation to the position of detector arrays. Even though absorption effects in the shallow detection geometry are much smaller than those in the grazing incidence geometry, and such effects can still be seen in the data. These cannot be simulated with LCF easily. We introduced a Au_2S contribution in the fit as a compensation for absorption effects, which proved to improve the resulting statistical fit significantly. Moreover, the contribution of Au_2S was steady over the angular scan, supporting a likely source of absorption effect. LCF results match the expected depth profiles for both Au(0) and Au(III) species, demonstrating as a first proof of principle the possibility to detect the change in gold species in depth. With the aid of LCF, the correct trend is visible, indicating that the method works successfully.

The replica sample S1 (Fig. 5b) is composed of a gold leaf applied over NGG-1b on top of α-Fe_2O_3 layer supported over gypsum. Since the uppermost layer is metallic gold and the NGG-1b directly underneath is also a Au(0)-species, a higher Au(0) signal is expected at the surface and near surface layers. It is to be kept in mind that NGG-1b has a very low gold

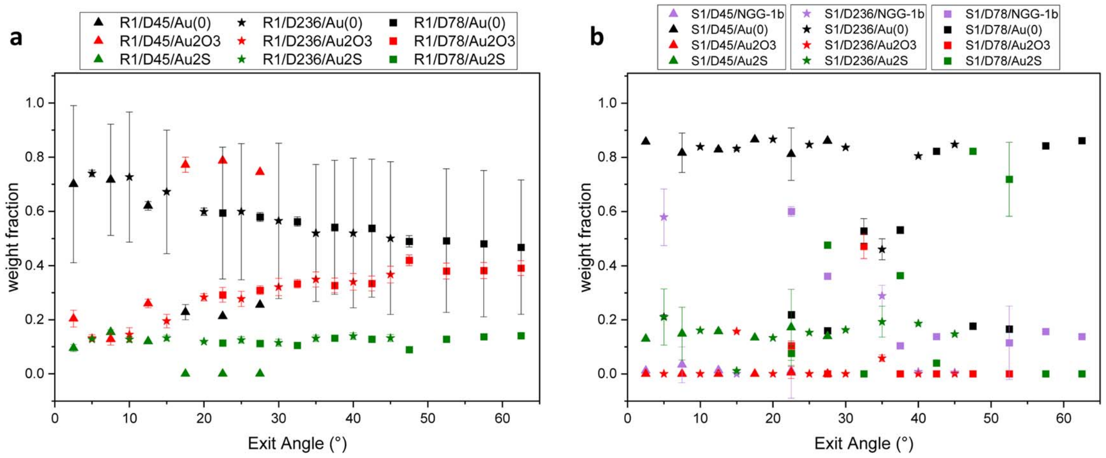

Fig. 5 Angular dependence of gold speciation as obtained from LCF of simultaneous Au L_3 AR-XANES from the three sets of detector arrays for (a) reference sample R1 and (b) replica sample S1. Black represents Au(0), red: Au_2O_3, green: Au_2S, and purple represents Nanogold Gel NGG-1b.

concentration compared to the above-mentioned 200 nm-thick gold layer.

Fig. 5b shows angular profiles of gold species weight fractions as obtained from LCF results. This include Au(0), NGG-1b, Au(III) oxide, and Au(I) sulfide species. The general trend of Au(0) and Au(III) species indicates almost steady concentration with the depth. Despite minor differences, the NGG-1b XANES spectrum is similar to that of Au(0) (compare Fig. 1b). This makes it harder to distinguish between both in the LCF process. Therefore, no information can be concluded about the presence or interaction of NGG-1b at the surface and near-surface layers. The major contribution of Au(0) species remains at the surface and near-surface layers and in average it remains almost constant as the detection angle increases. Negligible amounts of Au_2O_3 species in S1 are seen in trace amounts at all depths.

It is important to mention that Au(III) oxide undergoes photoinduced reduction at room temperature and pressure. To get a better idea about the rate of photoinduced reduction of Au(III) oxide, we performed a monitoring experiment (see ESI†) and noticed 26% decrease in Au(III) weight fraction and 74% increase of Au(0) fraction over the experiment time (800 minutes). After 80 minutes of one complete XANES measurement, almost 5% of Au(III) oxide was reduced (see ESI†). The reduction can go through Au(I) species before it is fully reduced to Au(0), hence we detect it in the LCF.

Influence of Au(III) species in NGG on AR-XRF measurements

The previous investigations of the AR-XANES spectra by LCF showed that a separation between Au(0) and Au(III) containing layers in the investigated sample is in principle possible. For the replica sample S1, Au(III) from the NGG could not be detected with certainty.

Therefore, another approach using forward simulations of the extracted AR-XRF signals is proposed to take a step towards quantitative depth profiling of the gold species. To mitigate the effects of systematic uncertainties from the solid angle of detection and (partly) sample inhomogeneity, relative intensity ratios are considered. The first intensity ratio labeled "Au(III)/ΣAu" was calculated by dividing the measured Au L_α intensity when the sample is excited by 11 922.5 eV photons (marker energy for Au(III)) with the Au L_α intensity when the sample is excited by 12 100 eV (marker energy for Au(0)). Thus, this signal reflects the contribution of Au(III) to the signal. The second ratio labeled "Au(0)/ΣAu" uses the Au L_α fluorescence signal obtained by excitation with 11 948.5 eV accordingly and reflects the signal originating from Au(0). It needs to be stressed that, of course, contributions to the fluorescence intensity of all gold species are present in both ratios, as clearly seen in the respective FY-XANES spectra of the reference compounds (Fig. 1). Those ratios are plotted in Fig. 6 for both, the reference sample R1 and the replica sample S1. With some similarity to the plots in Fig. 5, the ratios show almost constant behaviour except for Au(III)/ΣAu for the reference sample. Here, a steady increase is visible, resulting from the increase in information depth and thus Au(III) signal from the substrate.

The expected AR-XRF curves can be calculated using a model of the sample and the Sherman equation. The applied model of R1 consists of a pure Au layer on top of a mixture of Au_2O_3, Fe_2O_3 and cellulose with weight ratios of 19.8 wt%, 0.99 wt% and 79.2 wt% and a density of 19.32 g cm^{-3} for pure Au and 3.49 g cm^{-3} for the compound layer. S1 was produced from a Au layer on top of the NGG. The latter is modelled as $C_{102}H_{151}O_{39}N_{39}Au_{100}$ with a density of 1.742 g cm^{-3}. Due to the rough interfaces, no interference effects of the fluorescence radiation are expected (in contrast to GE-XRF). Therefore, no reflection and refraction is considered in the simulation. Since secondary excitation from the sample layers beneath the gold-containing layers is also unlikely, those layers can be neglected in the XRF calculation. The XRF intensities are calculated using the Sherman equation for primary radiation in a simplified form for both samples:

$$I(E) = \sum_{i=1,2} T_i^{\text{in}} T_i^{\text{out}} c_{\text{Au},i} \tau_{\text{Au},i}(E) \frac{1 - \exp\left(-\mu_i^*(E)\rho_i d_i\right)}{\mu_i^*(E)}$$

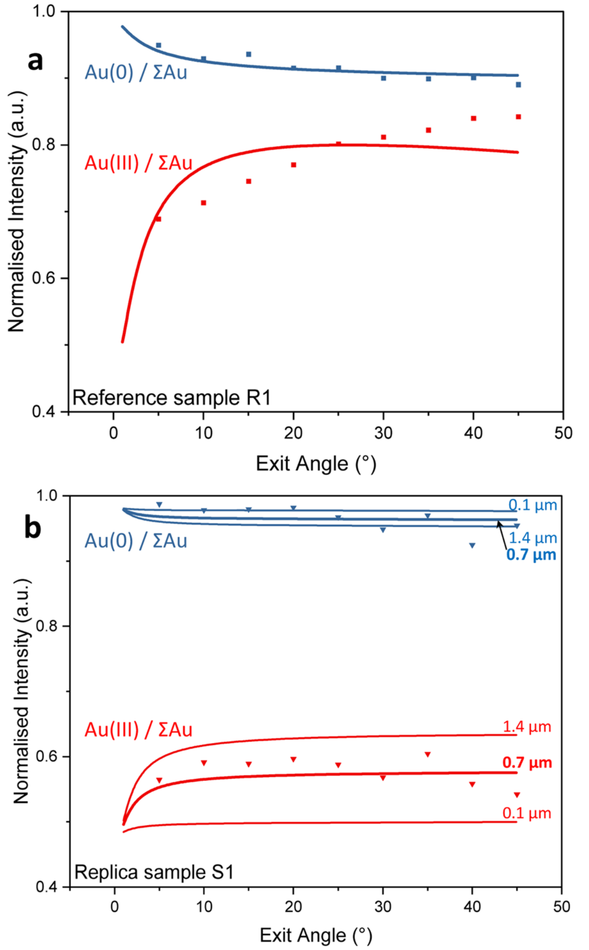

Fig. 6 Calculated (lines) and measured (symbols) relative intensities for Au(0) (blue) and Au(III) (red) in (a) reference sample R1 and (b) replica sample S1.

with $I(E)$ being the simulated fluorescence intensity for a given excitation energy E, $c_{\mathrm{Au},i}$ the mass fraction of Au, $\tau_{\mathrm{Au},i}$ the subshell ionization cross-section of Au in layer i, ρ_i the density and d_i the thickness of layer i, respectively. Moreover, the attenuation of the excitation beam and of the fluorescence radiation in layers above layer i must be taken into account, which is indicated with the transmission factors T_i^{out} (which are zero for i = 1). The composite attenuation coefficient μ_i is defined as follows:

$$\mu_i^*(E) = \frac{\mu_i(E)}{\sin(90^\circ - \theta_\mathrm{E})} + \frac{\mu_i(E_{\mathrm{Au\ L_3-M_5}})}{\sin(\theta_\mathrm{E})}$$

where μ_i is the attenuation coefficient of layer i and θ_E is the exit angle of the X-ray fluorescence with respect to the sample surface. Thus, the measured ratios are described by Au(*III*)/ΣAu = $A_{\mathrm{III}}I(11\,922.5\ \mathrm{eV})/I(12\,100\ \mathrm{eV})$ and Au(0)/ΣAu = $A_0 I(11\,948.5\ \mathrm{eV})/I(12\,100\ \mathrm{eV})$, with intensity factors A_{III} and A_0 discussed below.

Besides Au mass fractions and inter layer attenuation from other elements, the major impact on the simulated AR-XRF profiles of Au L_α originates from the subshell ionization cross-sections. Those are strongly different for the different Au species, as can be seen from the XANES spectra in Fig. 1. To include the fine structure into the simulation, the tabulated subshell ionization cross sections[37] used for the calculation are modified by factors 0.657 and 1.273 for Au(0) and Au(III) at 11 922.5 eV excitation and factors 1.062 and 0.979 for Au(0) and Au(III) at 12 948.5 eV excitation energy. For 12 100 eV excitation energy, the tabulated values are used. Note, also $\mu_{\mathrm{Au},i}$ is modified in the simulation according to the XANES fine structure, since it includes the sub-shell ionization cross-section. This, in turn, affects the absorption of incident radiation in upper layers as well.

Fig. 6 shows the comparison of the measured Au L_α AR-XRF ratios and simulated ones. To match the simulated and the measured curves, intensity factors $A_0 = 0.701$ and $A_{\mathrm{III}} = 0.894$ as well as a Au foil thickness of 200 nm have been chosen for both samples. For the thickness of the NGG layer for the replica sample, simulations for 1.4 µm, 0.7 µm and 0.1 µm are shown. As can be seen, the different NGG thicknesses have the greatest influence on the Au(III)/ΣAu ratio with a qualitatively best match of 0.7 µm with the data. For now, the obtained results do not fully explain the measured data, and thus, lack the quality necessary for truly quantitative significance. Repeated measurements on additional sample systems, *e.g.* with a variation of the gold foil thickness and Au(III) containing layer, would be necessary. Nevertheless, the simulations also indicate that the method's sensitivity is sufficient to detect the formation of Au(III) species in NGG with sub-micrometer thicknesses.

Discussion

While being an interesting result and hint for future analysis, there are several issues with the current data that need to be addressed here.

First of all, the origin of the necessary intensity factors is not clear. By taking the ratios of the normalized measured fluorescence intensities, major (angle-dependent) contributions to the fluorescence intensities like solid angle of detection, some uncertainties in the fundamental parameters and sample coverage cancel out. Moreover, many energy-dependent contributions are very similar for the three excitation energies (polycapillary lens efficiency, absorption of the excitation beam in the environment, and detection efficiency), due to the limited energy range. Finally, the simulation is considering all possible absorption effects within the sample, so that no intensity factors should have been necessary.

To double-check the assumptions made in the simulation and their effect on the intensity ratios, the influence of the sample parameters (density, composition) has also been checked but was found to be negligible. Of course, a major influence is the choice of subshell ionization cross-sections. Here, we tried to use a nonlinear fit approach to describe the measured curves. Indeed, the best-fit results showed a good agreement with the measured data, but the found subshell ionization cross-sections with values being off by up to 33% with respect to the XANES measurements seem to be unjustified. Therefore, we only state here the very conservative estimate of a detection limit in the several hundred nanometers up to micrometer range for Au(III) NGG.

The current research is meant to be a proof of principle; however, repeated measurements would have provided better statistics. The long measurement time needed for a complete XANES scan at all angles, and the limited beamtime did not allow for repeated measurements at different points. Additionally, surface irregularities of the samples made it difficult to find another spot within the limited beamtime.

It is important to report the experimental challenges faced during surface-sensitive analysis of lab-produced samples:

- A large flat even surface is difficult to obtain at the micrometer and sub-micrometer scales using wall painting pigments and plaster materials. This directly affects the detected fluorescence originating from the angular-dependent probed depth.
- Inhomogeneity of composition's spatial distribution in manually prepared samples and in historical wall painting samples. This leads to variation in thickness and density of the investigated volume and layer. This directly impacts the detected fluorescence intensity and any quantification based on it.
- The relatively very thin layer of NGG which provides very low Au concentration. This would make longer measurement times necessary, which in turn influences the chemical speciation of gold in the analysed position (radiation damage).
- The angular step-size was large to overcome surface roughness. For a smoother surface, angular scan with 0.01° step size using our setup is recommended to obtain a more precise and accurate chemical speciation in-depth.

In all cases, for a more even surface, angular scan with a maximum of 0.01° step size is recommended to decipher changes in chemical speciation with higher precision and accuracy. A few general observations from angular-dependent fluorescence profiles can be made:

- Near-surface and sub-surface layers can be investigated with AR-XANES. Improved surface smoothness enhances the success of the investigation.
- Chemical speciation in depth using AR-XANES at marker energies is informative about stratigraphic chemical composition non-destructively and non-invasively.
- Using the non-invasive and non-destructive grazing exit setup, it is possible to distinguish the reaction of a nanogold material underneath a bulk gold layer of 200 nm thickness.

The method has an unequivocal advantage of being non-destructive and non-invasive at room temperature and pressure, in contrast to many other methods such as Secondary Ion Mass Spectrometry (SIMS), Electron Energy-Loss Spectroscopy (EELS), and powder X-Ray Diffraction (pXRD). No invasive sampling is needed, and limited radiation damage is monitored for the analysed sample. Importantly, the impact of synchrotron radiation on the analysed materials is recommended to be tested in advance. While surface zero roughness remains ideal, the necessity of having a smooth surface to successfully perform this experiment is unquestionable.

Application of this technique on cultural heritage samples or further development into a quantitative method includes additional technical challenges. For example, partial knowledge about sample composition and structure of the heritage sample (stratigraphic information), complex composition (original, altered, or added materials; heterogeneous density distribution; heterogeneous crystalline phases and distribution), variable thickness for individual layers within one sample and multiple samples of one object or type of heritage material (ranging from nanometers to micrometers), flat smooth surface at the microscale for the analysed heritage sample, in addition to sample's integrity where non-destructive and non-invasive approach is prioritised, including avoiding any radiation damage.

Another experimental challenge when dealing with actual historical samples, depending on the condition of gold layer, the density of the gold layer may change. Partial and complete oxidation are both possible, in addition to physical losses in the gold layer generating heterogeneous and discontinuous layer of the metal leading to different densities at different analysed points. The impact would provide erroneous fitting of calculated profiles. Therefore, a 3D elemental map of the analysed surface would then be beneficial to precede the calculations.

Conclusions

AR-μXANES allows qualitative and quantitative analyses. However, quantification was not approached at this stage of our work.

The designed experimental constellation is innovative and new, we presented our AR-XANES/AR-XRF investigation method and results as applied for non-destructive characterising chemical speciation in depth for cultural heritage. Further improvements on this setup and tested samples are possible and envisaged. Application fields for this setup are inclusive for other non-destructive and non-invasive applications. Our work here is accomplishing new frontiers in investigating nano and atomic scales of a remedial intervention. To the best of our knowledge, no earlier heritage science research questioned the chemical interaction between binder-support. Our research in its tools and findings increases our understanding about this interaction and opens new research possibilities at this front.

Further improvements on this setup and tested samples are possible and envisaged. Application fields for this setup are inclusive for all non-destructive and non-invasive investigations and the method remains unrestricted to cultural heritage materials. Photovoltaic samples, polymers, modern paints, industrial coatings, and electronics, to mention some examples, can benefit from this technique.

This research gives a first integrated plan on assessing a conservation material at surface and interfaces. More studies focusing on unexplored areas in this research such as long-term use of NGG for gilded paintings or improved NGG, can now follow. Thinking outside the box and making conservation decisions that are unconventional should not be avoided. Every heritage object is unique by itself. And there are common conservation phenomena that can be treated using what is now known as conventional materials and methods but used to be once new and unconventional. The same applies today and here, delivering a new way of thinking by bringing a new compatible conservation material and a new investigation method that may be considered conventional in the future.

Data availability

The data supporting this article have been included as part of the ESI.†

Author contributions

Maram Na'es: conceptualization, methodology, replica preparation, formal analysis, data treatment, figure preparation, writing the original draft and editing. Lars Lühl: conceptualization, methodology, formal analysis, review and editing. Daniel Grötzsch: methodology, formal analysis. Ioanna Mantouvalou: methodology, review and editing. Jonas Bauman: theoretical calculations, writing and editing. Birgit Kanngießer: funding and review.

Conflicts of interest

The authors have no conflicts of interest to declare.

Acknowledgements

Measurements were carried out at the MySpot beamline at the BESSY II electron storage ring operated by the Helmholtz-Zentrum Berlin für Materialien und Energie. We would like to thank Dr Ivo Zizak for assistance during the experiment. Financial support from the German Research Foundation 'DFG', project number 285789434, is gratefully appreciated.

References

1 A. Burnstock, K. J. van den Berg, S. de Groot and L. Wijnberg, *Modern Paints Uncovered*, 2003, pp. 6–8.

2 M. Na'es, *et al.*, Synthesis and characterisation of a novel nano gold material for the conservation of cultural heritage, in *European Conference on X-Ray Spectrometry*, Bologna, Italy, 2014, pp. 15–20.

3 V. Graziani, M. Iorio, M. Albini, C. Riccucci, G. Di Carlo, P. Branchini, *et al.*, Metals and Environment: Chemical Outputs From the Interaction Between Gilded Copper-Based Objects and Burial Soil, *Front. Mater.*, 2020, 7(February), 1–9.

4 I. Val'syunas, P. Mechinskas, V. Yasulaitene and K. Leinartas, Initial stages of the copper corrosion in sulfite-containing solutions, *Prot. Met.*, 2002, **38**(1), 71–77.

5 M. Na'es, Analytical Investigations and Conservation of Nabataean Gilded Wall Paintings, PhD dissertation, Technical University, Berlin, 2024.

6 N. C. Schellmann, Animal glues: a review of their key properties relevant to conservation, *Stud. Conserv.*, 2007, **52**(suppl. 1), 55–66.

7 T. H. Hsieh, A. J. Kinloch, K. Masania, A. C. Taylor and S. Sprenger, The mechanisms and mechanics of the toughening of epoxy polymers modified with silica nanoparticles, *Polymer (Guildf)*, 2010, **51**(26), 6284–6294, DOI: 10.1016/j.polymer.2010.10.048.

8 M. Shah, V. Badwaik, Y. Kherde, H. K. Waghwani, T. Modi, Z. P. Aguilar, *et al.*, Gold nanoparticles: Various methods of synthesis and antibacterial applications, *Front. Biosci.*, 2014, **19**(8), 1320–1344.

9 M. Harada and S. Kizaki, Formation Mechanism of Gold Nanoparticles Synthesized by Photoreduction in Aqueous Ethanol Solutions of Polymers Using In Situ Quick Scanning X-ray Absorption Fine Structure and Small-Angle X-ray Scattering, *Cryst. Growth Des.*, 2016, **16**(3), 1200–1212.

10 E. Pouyet, B. Fayard, M. Salomé, Y. Taniguchi, F. Sette and M. Cotte, Thin-sections of painting fragments: Opportunities for combined synchrotron-based micro-spectroscopic techniques, *Heritage Sci.*, 2015, **3**(1), 1–16.

11 V. A. Solé, E. Papillon, M. Cotte, P. Walter and J. Susini, A multiplatform code for the analysis of energy-dispersive X-ray fluorescence spectra, *Spectrochim. Acta, Part B*, 2007, **62**(1), 63–68.

12 M. Cotte, J. Susini, V. A. Solé, Y. Taniguchi, J. Chillida, E. Checroun, *et al.*, Applications of synchrotron-based micro-imaging techniques to the chemical analysis of ancient paintings, *J. Anal. At. Spectrom.*, 2008, **23**(6), 820–828.

13 G. van der Snickt, K. Janssens, J. Dik, W. De Nolf, F. Vanmeert, J. Jaroszewicz, *et al.*, Combined use of Synchrotron Radiation Based Micro-XRF, Micro-XRD, Micro-XANES and Micro-FTIR for Revealing an Alternative Degradation Pathway of the Pigment Cadmium Yellow in a Painting by Van Gogh, *Anal. Chem.*, 2012, **84**(23), 10221–10228.

14 A. Lluveras, S. Boularand, J. Roqué, M. Cotte, P. Giráldez and M. Vendrell-Saz, Weathering of gilding decorations investigated by SR: Development and distribution of calcium oxalates in the case of Sant Benet de Bages (Barcelona, Spain), *Appl. Phys. A:Mater. Sci. Process.*, 2008, **90**(1), 23–33.

15 G. Van Der Snickt, C. Miliani, K. Janssens, B. G. Brunetti, A. Romani, F. Rosi, *et al.*, Material analyses of "Christ with singing and music-making Angels", a late 15th-C panel painting attributed to Hans Memling and assistants: Part I. Non-invasive in situ investigations, *J. Anal. At. Spectrom.*, 2011, **26**(11), 2216–2229.

16 L. Monico, F. Rosi, C. Miliani, A. Daveri and B. G. Brunetti, Non-invasive identification of metal-oxalate complexes on polychrome artwork surfaces by reflection mid-infrared spectroscopy, *Spectrochim. Acta, Part A*, 2013, **116**(2013), 270–280, DOI: 10.1016/j.saa.2013.06.084.

17 L. Bertrand, M. Cotte, M. Stampanoni, M. Thoury, F. Marone and S. Schöder, Development and trends in synchrotron studies of ancient and historical materials, *Phys. Rep.*, 2012, **519**(2), 51–96, DOI: 10.1016/j.physrep.2012.03.003.

18 M. Cotte, J. Susini, J. Dik and K. Janssens, Spectroscopy for Art Conservation : Looking Back, *Acc. Chem. Res.*, 2010, **43**(6), 705–714, http://www.ncbi.nlm.nih.gov/pubmed/20058906.

19 L. Lühl, I. Mantouvalou, W. Malzer, I. Schaumann, C. Vogt, O. Hahn, *et al.*, Reconstruction procedure for 3D micro X-

ray absorption fine structure, *Anal. Chem.*, 2012, **84**(4), 1907–1914.

20 L. Lühl, B. Hesse, I. Mantouvalou, M. Wilke, S. Mahlkow, E. Aloupi-Siotis, *et al.*, Confocal XANES and the attic black glaze: The three-stage firing process through modern reproduction, *Anal. Chem.*, 2014, **86**(14), 6924–6930.

21 M. Na'es, L. Lühl, T. Wolff and B. Kanngießer, Technical study of Jordanian wall paintings from Petra using SR 3D-μXANES and 3D-μXRF, in *SESAME 8th Natl Users Meeting*, 2012.

22 C. T. Çakir, T. Piotrowiak, U. Reinholz, A. Ludwig, F. Emmerling, C. Streli, *et al.*, Exploring the Depths of Corrosion: A Novel GE-XANES Technique for Investigating Compositionally Complex Alloys, *Anal. Chem.*, 2023, **95**(10), 4810–4818.

23 J. Orsilli, A. Migliori, R. Padilla-Alvarez, M. Martini and A. Galli, AR-XRF measurements and data treatment for the evaluation of gilding samples of cultural heritage, *J. Anal. At. Spectrom.*, 2023, 174–185.

24 Y. Kayser, J. Szlachetko and J. Sà, Scanning-free grazing emission X-ray fluorescence by means of an angular dispersive arrangement with a two-dimensional position-sensitive area detector, *Rev. Sci. Instrum.*, 2013, **84**(12), 1–11.

25 J. Baumann, Y. Kayser and B. Kanngießer, Grazing Emission X-Ray Fluorescence: Novel Concepts and Applications for Nano-Analytics, *Phys. Status Solidi B*, 2021, **258**(3), 1–17.

26 F. Meirer, G. Pepponi, C. Streli, P. Wobrauschek and N. Zoeger, Grazing exit versus grazing incidence geometry for X-ray absorption near edge structure analysis of arsenic traces, *J. Appl. Phys.*, 2009, **105**(7), 074906.

27 K. Tsuji, Z. Spolnik, K. Wagatsuma, S. Nagata and I. Satoh, Grazing-exit x-ray spectrometry for surface, and thin-film analyses, *Anal. Sci.*, 2001, **17**(1), 145–148.

28 K. Tsuji and F. Delalieux, Feasibility study of three-dimensional XRF spectrometry using μ-X-ray beams under grazing-exit conditions, *Spectrochim. Acta, Part B*, 2003, **58**(12), 2233–2238.

29 Y. Kayser, P. Hönicke, D. Banaś, J. C. Dousse, J. Hoszowska, P. Jagodziński, *et al.*, Depth profiling of low energy ion implantations in Si and Ge by means of micro-focused grazing emission X-ray fluorescence and grazing incidence X-ray fluorescence, *J. Anal. At. Spectrom.*, 2015, **30**(5), 1086–1099.

30 V. Szwedowski, J. Baumann, I. Mantouvalou, L. Bauer, W. Malzer and B. Kanngießer, Scan-Free Grazing Emission XRF Measurements in the Laboratory Using a CCD, *Phys. Status Solidi C*, 2017, **14**(12), 1–6.

31 ICOMOS, *ICOMOS Principles for the Preservation and Conservation-Restoration of Wall Paintings*, Zimbabwe, 2003, **https://www.icomos.org/images/DOCUMENTS/Charters/wallpaintings_e.pdf**.

32 F. Förste, L. Bauer, K. Heimler, B. Hansel, C. Vogt, B. Kanngießer, *et al.*, Quantification routines for full 3D elemental distributions of homogeneous and layered samples obtained with laboratory confocal micro XRF spectrometers, *J. Anal. At. Spectrom.*, 2022, **37**(8), 1687–1695.

33 B. Ravel and M. Newville, ATHENA, ARTEMIS, HEPHAESTUS: Data analysis for X-ray absorption spectroscopy using IFEFFIT, *J. Synchrotron Radiat.*, 2005, **12**(4), 537–541.

34 I. Zizak, mySpot: a versatile microfocussing station for scanning methods at BESSY II, *J. Large Scale Res. Facil.*, 2016, **2**, 1–10.

35 A. Erko and I. Zizak, Hard X-ray micro-spectroscopy at Berliner Elektronenspeicherring für Synchrotronstrahlung II, *Spectrochim. Acta, Part B*, 2009, **64**(9), 833–848, DOI: **10.1016/j.sab.2009.07.003**.

36 Lawrence Berkeley National Laboratory's (LBNL), *Materials Sciences Division (MSD)*, CXRO The Center for X-Ray Optics, 2019, **https://www.cxro.lbl.gov/**.

37 H. Ebel, R. Svagera, M. F. Ebel, A. Shaltout and J. H. Hubbell, Numerical description of photoelectric absorption coefficients for fundamental parameter programs, *X-Ray Spectrom.*, 2003, **32**(6), 442–451.